

Supporting Information

Engineering Mo/Mo₂C/MoC Hetero-interfaces for Enhanced Electrocatalytic Nitrogen Reduction

Ying Liu,^{†a} Xiaorong Zhu,^{†a} Qinghua Zhang,^c Tang Tang,^{b,d} Yun Zhang,^{b,d} Lin Gu,^c
Yafei Li,^a Jianchun Bao,^a Zhihui Dai,^{*a} Jin-Song Hu,^{*b,d}

^a *Jiangsu Collaborative Innovation Center of Biomedical Functional Materials, School of Chemistry and Materials Science, Nanjing Normal University, Nanjing 210023, China*

^b *Beijing National Laboratory for Molecular Sciences (BNLMS), CAS Key Laboratory of Molecular Nanostructure and Nanotechnology, Institute of Chemistry, Chinese Academy of Sciences, Beijing 100190, China*

^c *Beijing National Laboratory for Condensed Matter Physics, Institute of Physics, Chinese Academy of Sciences, Beijing 100190, China*

^d *University of the Chinese Academy of Sciences, Beijing 100049, China*

[†] *These authors contributed equally to this work.*

Corresponding Author

[*hujs@iccas.ac.cn](mailto:hujs@iccas.ac.cn)

[*daizhihui@njnu.edu.cn](mailto:daizhihui@njnu.edu.cn)

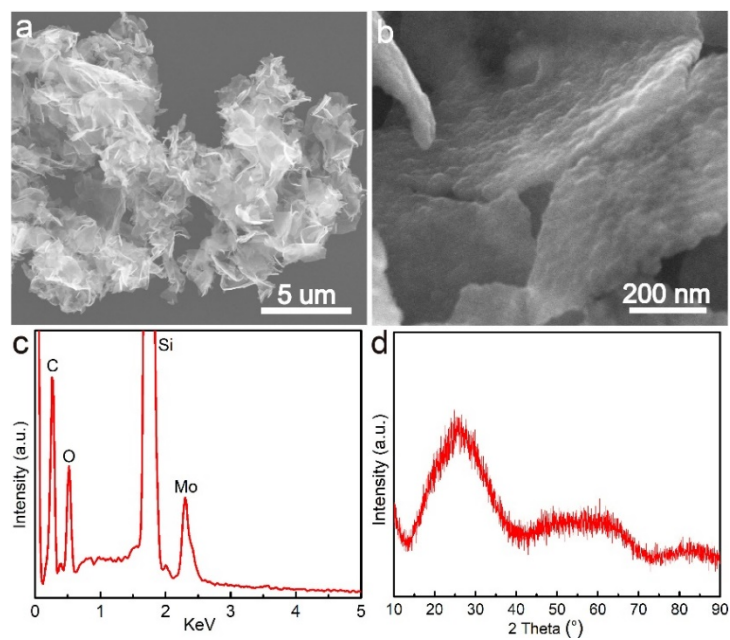


Figure S1. (a) Low- and (b) high-magnification SEM images, (c) EDS profile and (d) XRD pattern of the Mo-containing precursor.

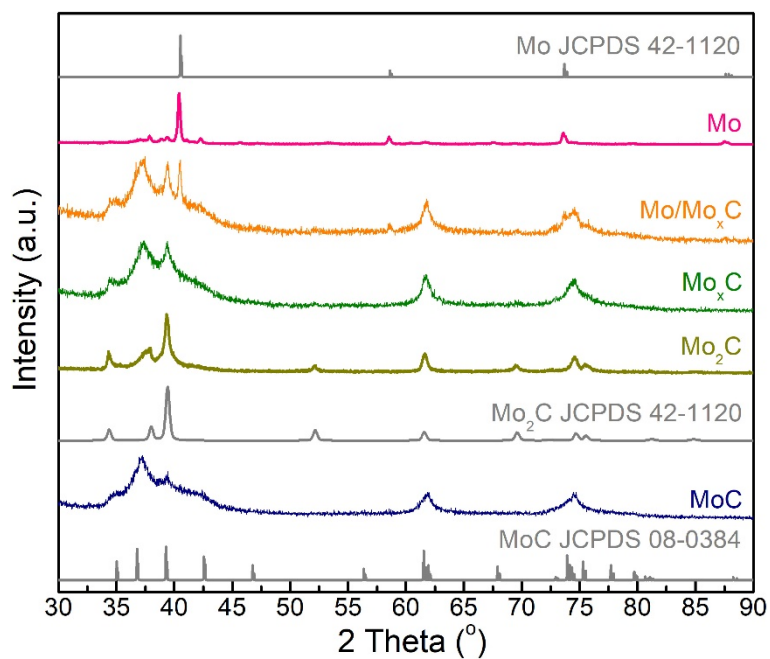


Figure S2. XRD patterns for MoC, Mo₂C, Mo_xC, Mo/Mo_xC and Mo samples.

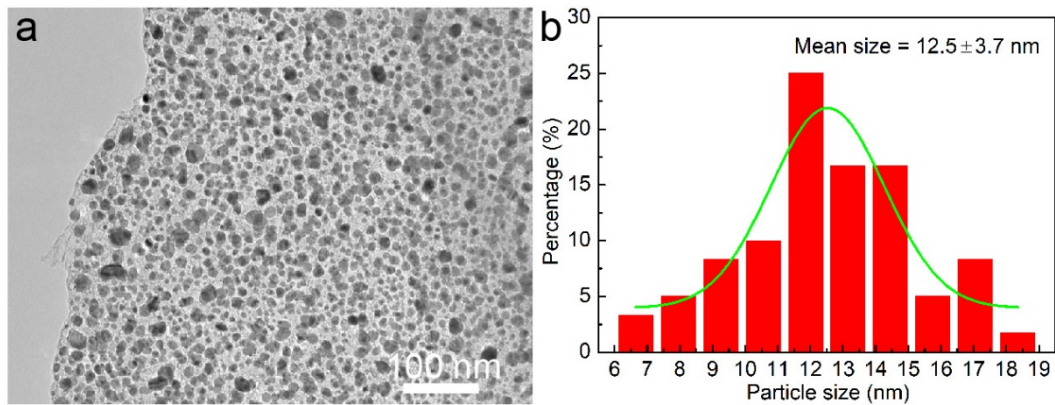


Figure S3. (a) TEM and (b) nanoparticles diameter distribution histogram for the Mo₂C sample.

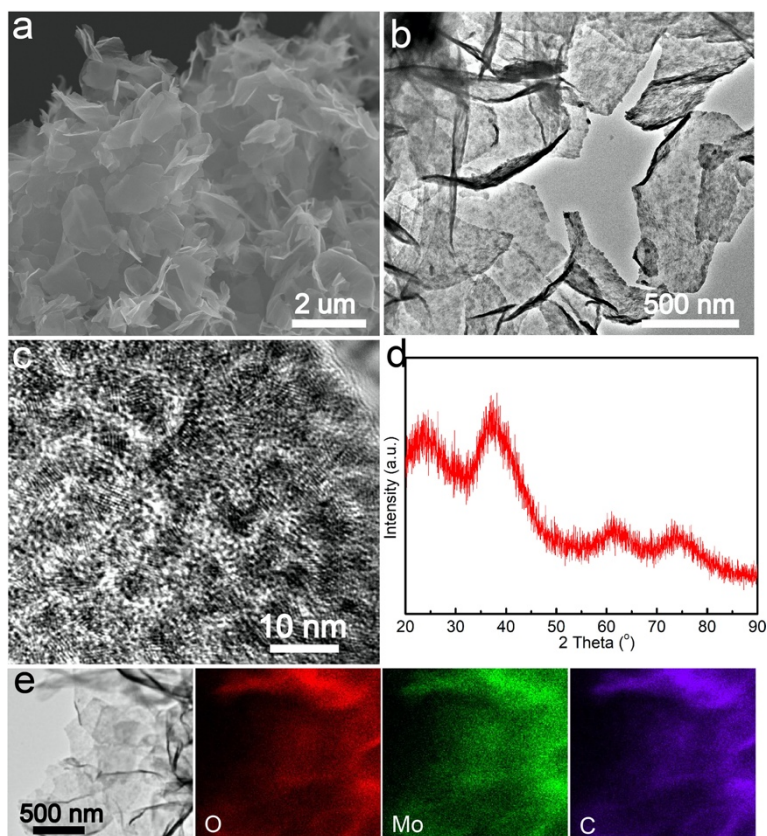


Figure S4. (a) SEM, (b) TEM and (c) high-magnification TEM, (d) XRD pattern and (e) EDS mapping images for the MoO_xC_y intermediate.

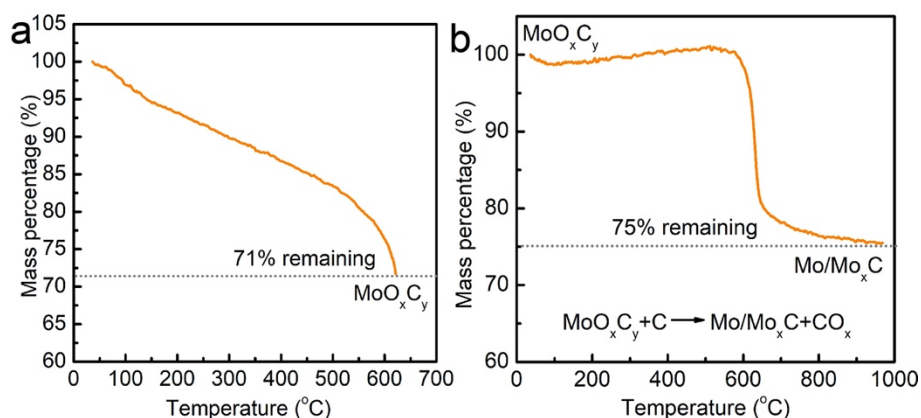


Figure S5. TGA profiles of (a) MoO_xC_y intermidate obtained from the annealing of polymer precursor at 650 °C, and (b) Mo/Mo_xC product obtained from the further annealing of MoO_xC_y at 1000 °C under N₂ flow.

In Figure S5a, the initial weight loss below 150 °C is ascribed to water evaporation. With the temperature gradually increases, the polymer precursor starts to decomposition along with the formation of MoO_xC_y. When the temperature exceeds 550 °C, a quick weight loss is observed due to the combustion of carbon. The remaining weight after heating to 650 °C is about 71%. In Figure S5b, solid state reaction between MoO_xC_y and carbon occurs accompanied by the carbonization and reduction, generating and releasing CO_x.

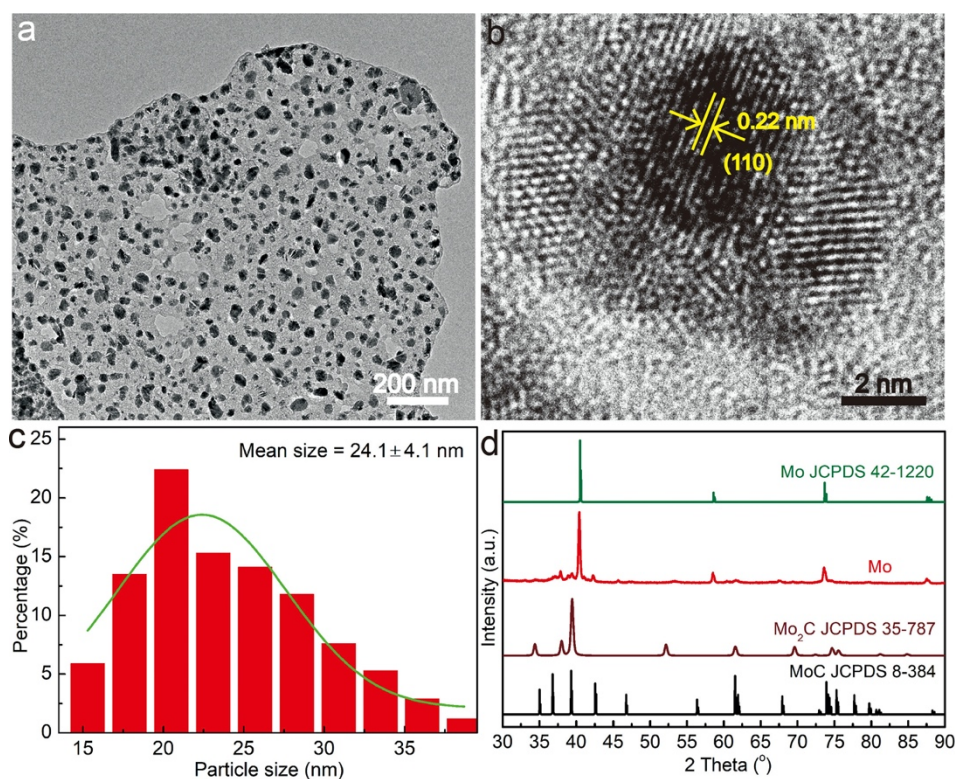


Figure S6. (a) TEM (b) HRTEM (c) nanoparticles size distribution histogram and (d) XRD pattern for the metallic Mo sample.

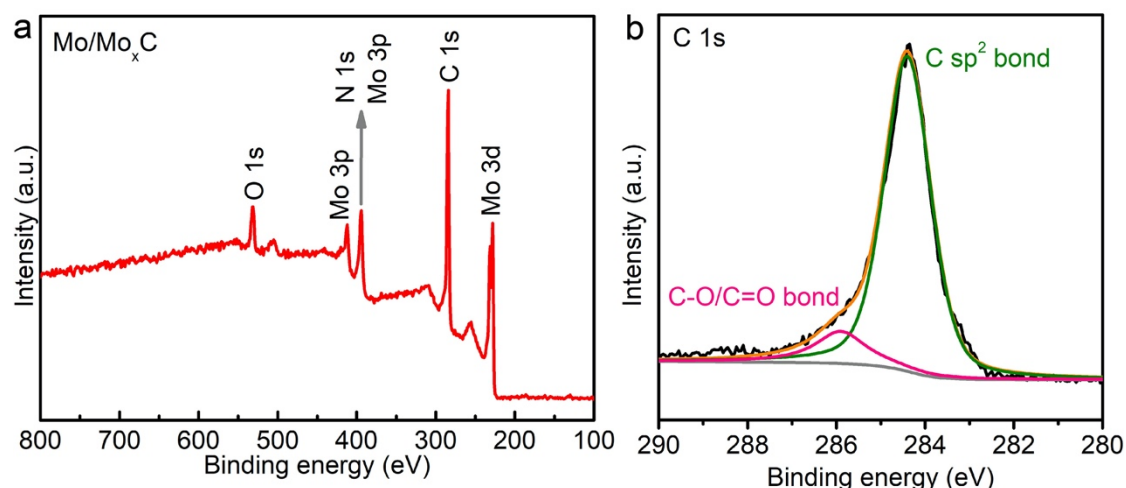


Figure S7. (a) Wide-scan survey, and (b) high-resolution C 1s XPS spectra for the Mo/Mo_xC sample.

Table S1. Fitting parameters for Mo signals in Mo/Mo_xC

<i>Valence state</i>	<i>BE (eV)</i>	<i>FWHM</i>	<i>Area</i>
<i>Mo</i>	228.0	0.68	11050.20
	231.2	0.85	9027.76
<i>Mo²⁺</i>	228.3	0.88	16508.61
	231.5	1.15	14053.62
<i>Mo⁴⁺</i>	229.2	1.74	8284.90
	232.3	1.10	3841.25
<i>Mo⁶⁺</i>	233.2	1.53	4348.37
	235.5	1.60	3468.00

Based on the fitted peak area of Mo and the total peak area of Mo 2p, the content of metallic Mo can be calculated as:

$$\frac{\text{peak area of Mo}}{\text{total peak area of Mo } 2p} = 0.28$$

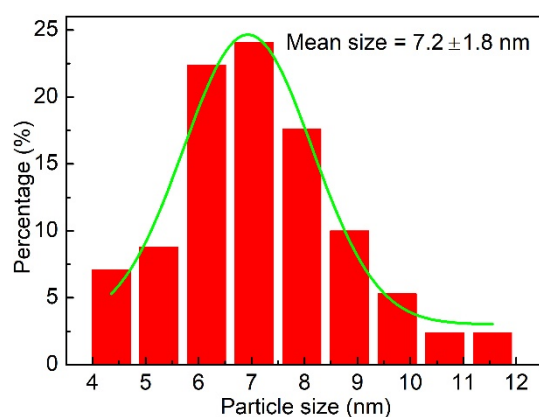


Figure S8. Nanoparticles diameter distribution histogram for the Mo/Mo_xC sample.

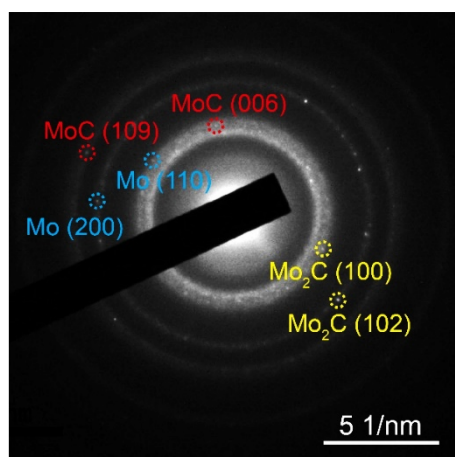


Figure S9. Selected area electron diffraction image for the Mo/Mo_xC sample.

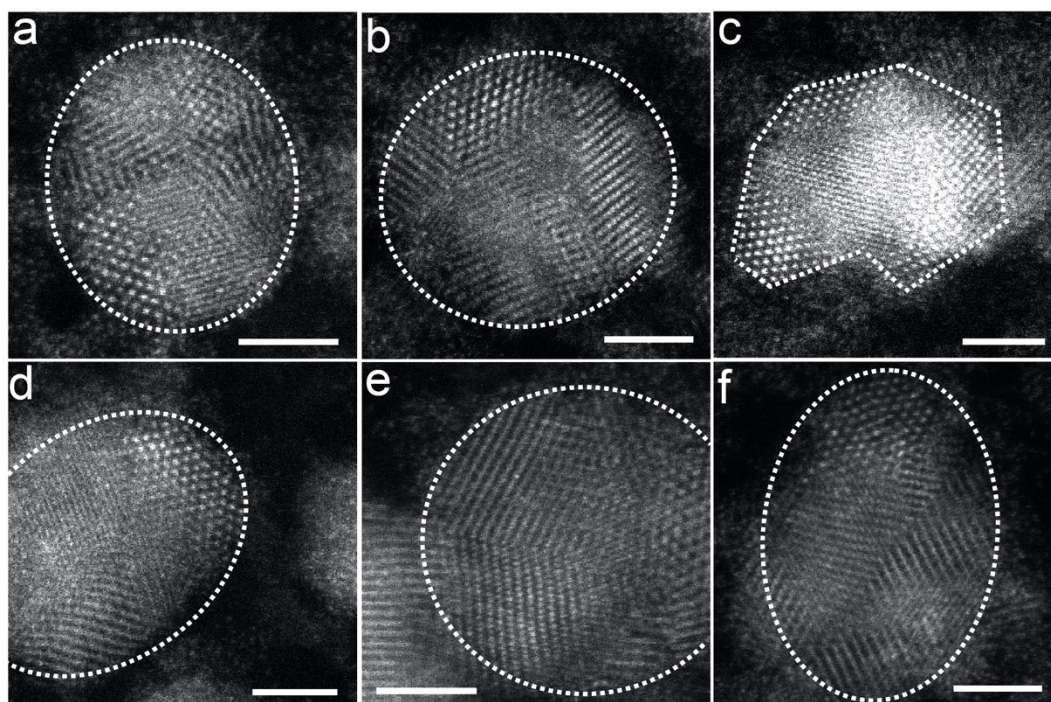


Figure S10. STEM images for the Mo/Mo_xC sample.

As shown in Figure S10, it is observed that nanoparticles are composed of different types of lattice fringes which can be indexed to MoC, Mo₂C, and metallic Mo, indicating the formation of heterostructured Mo/Mo_xC. Moreover, massive atomic deficiencies, grain boundaries and dislocations are also observed, especially on the heterogeneous interfaces.

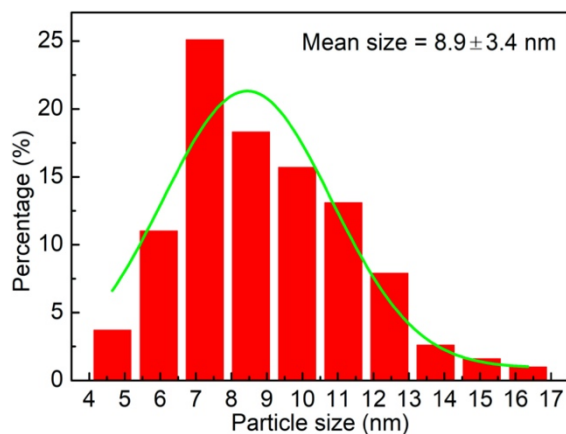


Figure S11. Nanoparticles diameter distribution histogram for the Mo_xC sample.

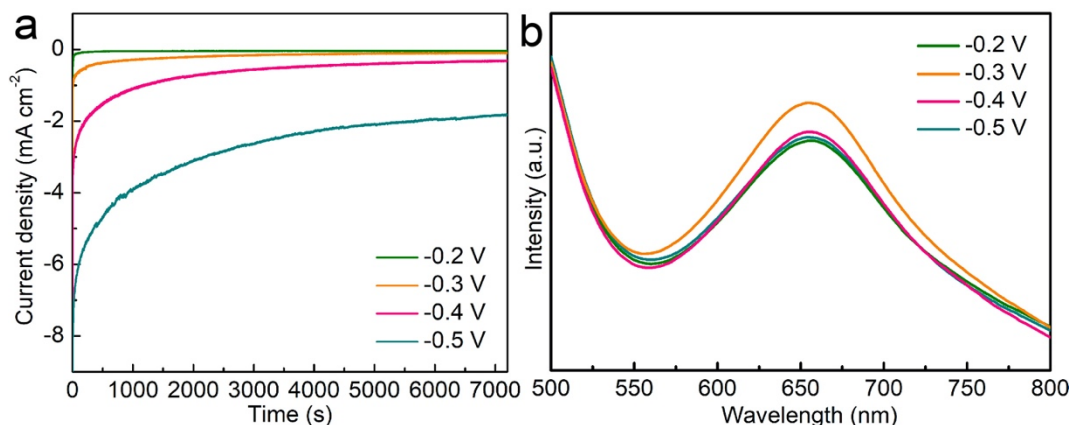


Figure S12. (a) Chronoamperometry curves and (b) UV-vis absorption spectra at each given potential for the $\text{Mo}/\text{Mo}_x\text{C}$ catalyst measured in 0.1 M Na_2SO_4 (the calibration curve used herein is $y=0.035x+0.0387$).

Figure S12a shows the chronoamperometric curves of the $\text{Mo}/\text{Mo}_x\text{C}$ catalyst. The current density increases in sequence as the applied potential increases from -0.2 V to -0.5 V (vs. RHE). Figure S12b shows the corresponding UV-Vis absorption spectra. The peak intensity at about 655 nm increases as the potential decreases from -0.5 V to -0.3 V, indicative of the increased NH_3 yield.

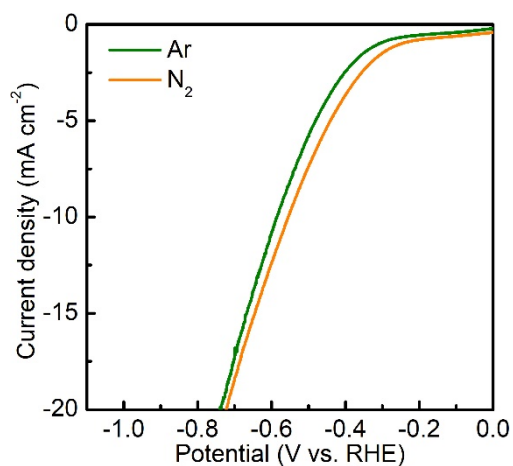


Figure S13. LSV curves recorded in N₂- and Ar-saturated electrolyte for the Mo/Mo_xC catalyst.

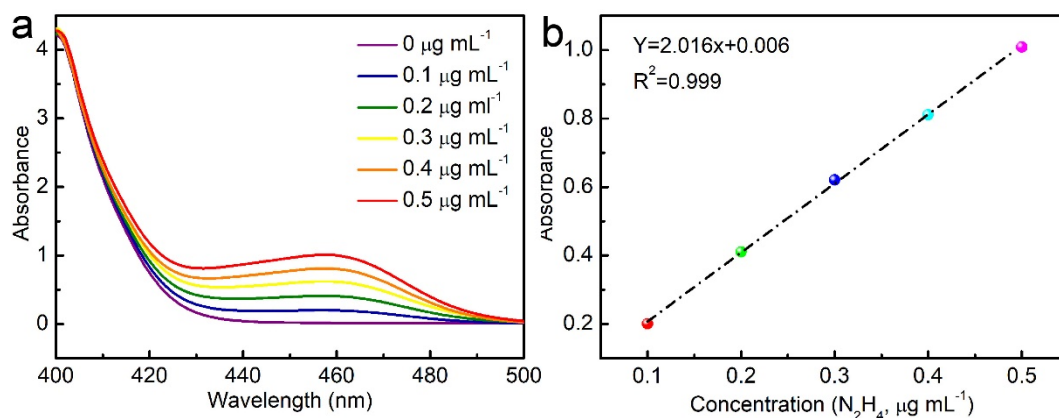


Figure S14. (a) UV-vis absorption spectra of 0.1 M Na₂SO₄ electrolyte with various N₂H₄ concentrations. (b) Calibration curve used for the calculation of N₂H₄ concentrations.

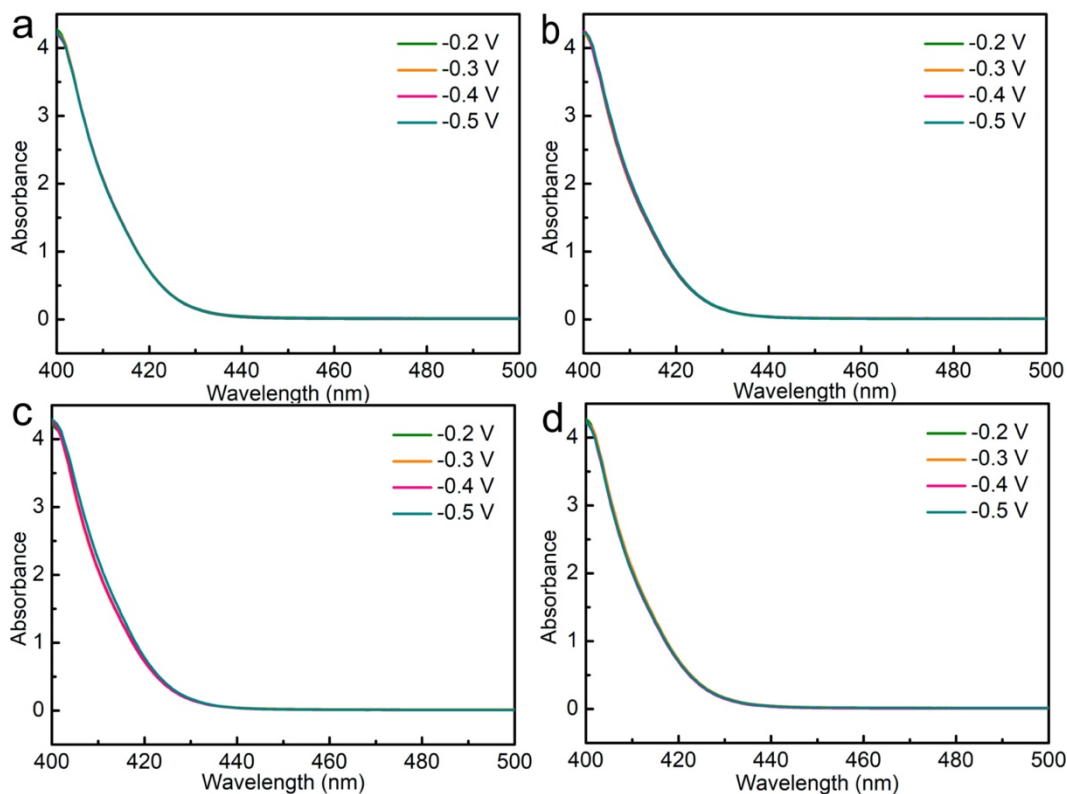


Figure S15. UV-vis absorption spectra of the electrolytes estimated by the Watt and Chrisp method for (a) Mo/Mo_xC, (b) Mo_xC, (c) metallic Mo, and (d) Mo₂C catalyst at different potentials.

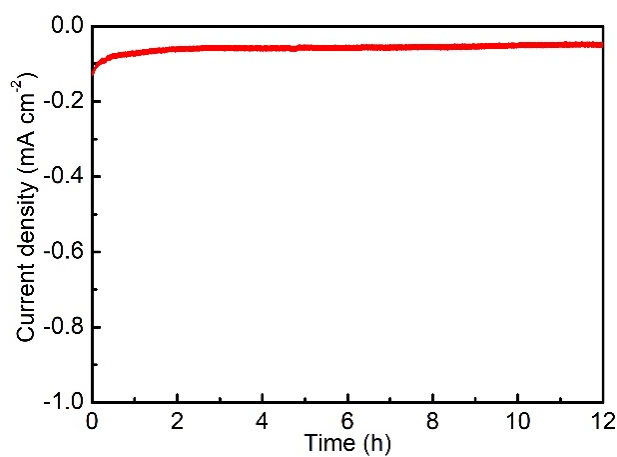


Figure S16. Chronoamperometric stability test (at -0.3 V vs. RHE) for the Mo/Mo_xC catalyst.

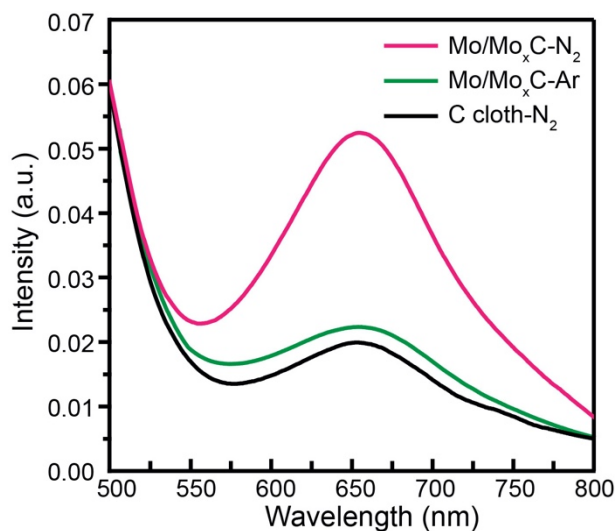


Figure S17. UV-vis absorption spectra of the cathode electrolytes stained with indophenol indicator after 2 h potentiostatic test at -0.3 V (vs. RHE) in 0.1 M Na₂SO₄ for bare carbon cloth measured in N₂-saturated atmosphere and carbon cloth with the Mo/Mo_xC catalyst measured in Ar- and N₂-saturated atmosphere.

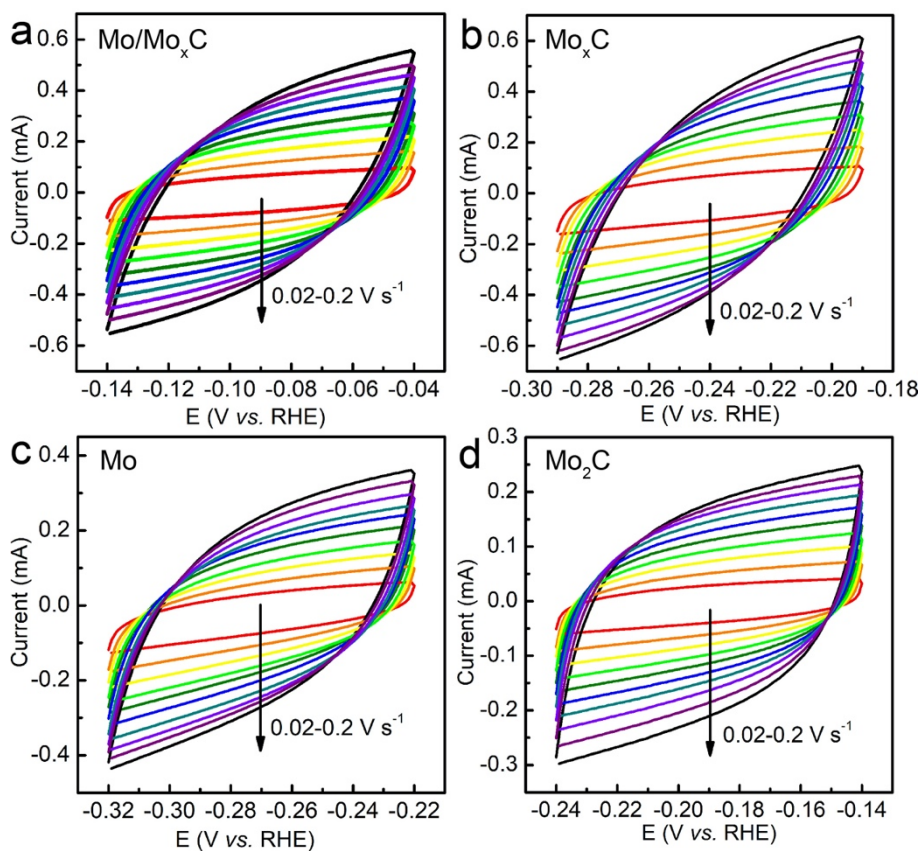


Figure S18. CV curves of (a) Mo/Mo_xC, (b) Mo_xC, (c) Mo, and (d) Mo₂C catalysts measured at scan rates from 20 to 200 mV s⁻¹.

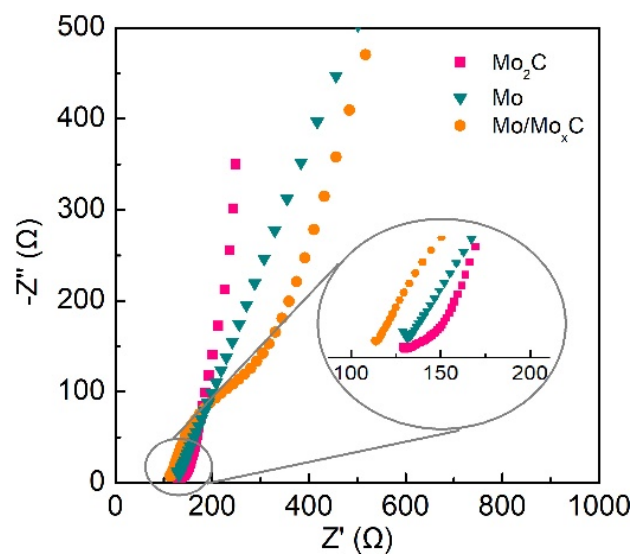


Figure S19. EIS Nyquist plots for the Mo, Mo₂C and Mo/Mo_xC catalysts measured in N₂-saturated 0.1 M Na₂SO₄ at a potential of -0.3 V (vs. RHE).

Table S2. Performance comparison of Mo-based and some precious-metal-based NRR electrocatalysts.

Catalyst	NH ₃ yield rate	FE (%)	electrolyte	Ref.
MoS₂/CC	4.94 μg h ⁻¹ cm ⁻² (-0.5 V vs. RHE)	1.17	0.1 M Na ₂ SO ₄	Adv. Mater., 2018, 30, 1800191.
Mo₂C/C	11.3 (-0.3 V vs. RHE)	7.8	0.5 M Li ₂ SO ₄	Adv. Mater., 2018, 30, 1803694.
MoO₃ nanosheet	29.43 (-0.5 V vs. RHE)	1.9	0.1 M HCl	J. Mater. Chem. A, 2018, 6, 12974.
(110)-oriented Mo	3.09 x 10 ⁻¹¹ mol s ⁻¹ cm ⁻² (-0.49 V vs. RHE)	0.72	0.5 M H ₂ SO ₄	J. Mater. Chem. A, 2017, 5, 18967.
SA-Mo/NPC	34.0 ± 3.6 μg h ⁻¹ mg ⁻¹ (-0.3V vs. RHE)	14.6 ±1.6	0.1 M KOH	Angew. Chem. Int. Ed, 2019, 58, 2321.
Au nanorod	1.648 μg h ⁻¹ cm ⁻² (-0.2V vs. RHE)	4.02	0.1 M KOH	Adv. Mater., 2017, 29, 1604799.
Au/CeO_x-RGO hybrid	8.3 μg h ⁻¹ mg ⁻¹ (-0.2 V vs. RHE)	10.10	0.1 M HCl	Adv. Mater., 2017, 29, 1700001.
Pd_{0.2}Cu_{0.8}/rGO composite	2.80 μg h ⁻¹ mg ⁻¹ (-0.2 V vs. RHE)	~	0.1 M KOH	Adv. Energy Mater., 2018, 8, 1800124.
Ru@ZrO₂/NC	3.7 mg h ⁻¹ mg _{Ru} ⁻¹ (-0.21 V vs. RHE)	21	0.1 M HCl	Chem, 2019, 5, 204-214.
Bi₄V₂O₁₁ /CeO₂	23.21 μg h ⁻¹ mg ⁻¹ (-0.2 V vs. RHE)	10.16	0.1 M HCl	Angew. Chem. Int. Ed., 2018, 57, 6073.
Fe₃O₄/Ti	5.6 × 10 ⁻¹¹ mol s ⁻¹ cm ⁻² (-0.4 V vs. RHE)	2.6	0.1 M Na ₂ SO ₄	Nanoscale, 2018, 10, 14386.
N-doped carbon/Fe₃C	15.804 μg h ⁻¹ mg ⁻¹ (-0.4 V vs. RHE)	2.72	0.1 M KOH	Catal. Sci. Technol., 2019, 9, 1208-1214.
Boron-Doped Graphene	9.8 μg h ⁻¹ cm ⁻² (-0.5 V vs. RHE)	10.8	0.05 M H ₂ SO ₄	Joule, 2018, 2, 1-13.
B₄C/CPE	26.57 μg h ⁻¹ mg ⁻¹ (-0.75 V vs. RHE)	15.95	0.1M HCl	Nat. Commun., 2018, 9, 3485.
Mo/Mo_xC	20.4 ug h ⁻¹ mg ⁻¹ (-0.3 V vs. RHE)	18.9	0.1 M Na ₂ SO ₄	This work